Mesoscale Structure in the Megalopolitan Snowstorm of 11–12 February 1983. Part I: Frontogenetical Forcing and Symmetric Instability

FREDERICK SANDERS

Center for Meteorology and Physical Oceanography, Massachusetts Institute of Technology, Cambridge, MA 02139

LANCE F. BOSART

Department of Atmospheric Science, State University of New York at Albany, Albany, NY 12222

(Manuscript received 11 May 1984, in final form 29 October 1984)

ABSTRACT

A cyclone moving northeastward off the coast of the northeastern United States on 11–12 February 1983 was accompanied by a band of heavy snow across all the major cities of this region from Washington to Boston. Frontogenetical forcing and symmetric instability are discussed as possible explanations of the intense precipitation. Rawinsonde data were analyzed to investigate the roles of these effects in this case. We found that intense ascent was part of a thermally direct transverse circulation, to be expected in response to frontogenetical forcing when the symmetric stability in the warmer air is small. Symmetric instability *per se* in the saturated major cloud mass may have been responsible for pulselike oscillations in its top. These were seen in satellite imagery, elongated in the direction of the tropospheric thermal wind.

1. Introduction

An intensifying cyclone moved northeastward from the vicinity of Cape Hatteras during 11–12 February 1983, the center passing some 300 km offshore from the south coast of New England. The synoptic situation is illustrated in Fig. 1. The storm produced abundant precipitation (Fig. 2), with a band of heavy snow from western North Carolina northeastward across or near every large city in the megalopolis extending from Washington to Boston. Needless to say, urban dislocation was great, as described in detail in *Storm Data* for this month.

An important aspect of the storm was the narrowness of the band of heavy snow. Its half-width (the lateral distance from the point of maximum fall to the point receiving half this amount) ranged from about 50 km in the North Carolina mountains to about 125 km in central Virginia to about 75 km in New England. These distances are clearly in the mesoscale range. In the southwest the distribution was no doubt strongly conditioned by orography, a matter which will not be addressed in this paper. In Virginia and Maryland substantial amounts of ice pellets and rain fell southeast of the region of maximum snow depth, as seen in Fig. 2a. Thus the total precipitation produced by the storm here was more broadly distributed. It is still seen that the locus of maximum snowfall and maximum precipitation were nearly coincident. In New England the precipitation was entirely in the form of snow in an unusually intense band lying at a typical distance northwest of the surface cyclone center (Brooks and Schell, 1950). We will here present evidence, derived mainly from analysis of rawinsonde data, that the concentration of precipitation was a manifestation of frontogenetical forcing within or adjacent to a region of small moist symmetric stability. Instability of this type may have occurred as well. A more detailed study of the situation in New England, based mainly on analysis of Doppler radar observations appears in Sanders and Bosart (1985). An investigation of an intense singular gravity wave, accompanied by thunderstorm activity as it propagated northeastward is presented in Bosart and Sanders (1985).

2. Physical mechanisms

The band of heavy snow was oriented approximately along the thermal wind (cf., Fig. 1). Such banded structure is a pervasive feature of cyclone-scale precipitation areas. Heymsfield (1979), Herzegh and Hobbs (1980) and Houze *et al.* (1981) have studied warm-front cases somewhat similar to the present one, but have addressed mainly the cloud-microphysical aspects. Two dynamical mechanisms that might be responsible for this phenomenon are frontogenetical forcing and symmetric instability.

The former was first empirically described by Bjerknes (1919) in terms of ascent of warm air over a wedge of cold air. Subsequent work by Namias and Clapp (1949), Sawyer (1956), Eliassen (1959) and

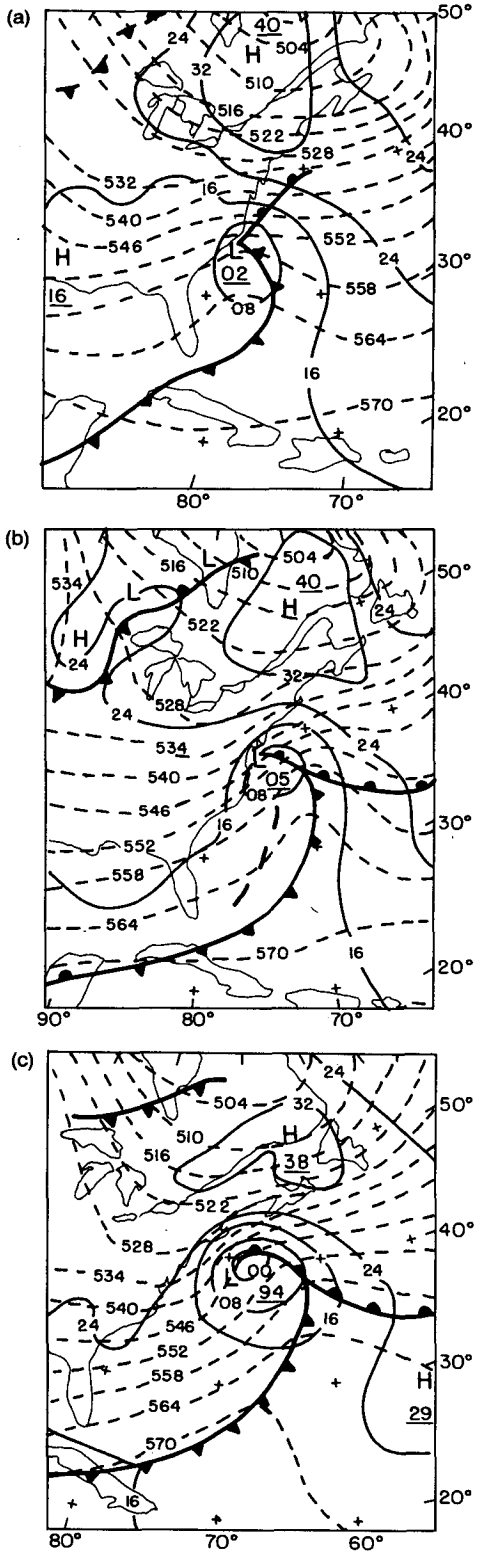

FIG. 1. Sea level isobars (solid lines, at intervals of 8 mb) and pressure centers, surface fronts (conventional notation) and thickness of the layer from 1000 to 500 mb (dashed lines, at intervals of 6 dam) for (a) 1200 GMT 11 February; (b) 0000 GMT 12 February; (c) 12000 GMT 12 February.

Hoskins and Bretherton (1972) has shown in physical terms how ascent of warm air and descent of cold air occurs. With large-scale geostrophic confluence acting to increase the horizontal temperature gradient by horizontal advection and to decrease the vertical wind shear by horizontal momentum advection, thermal-wind balance is upset. A thermally direct transverse circulation is induced to restore this balance, as sketched in Fig. 3a. The warm ascent is broad and gentle, and a discontinuity develops only at a boundary. Recent work by Emanuel (1985), however, shows that if the potential vorticity vanishes in the warm air, then the ascent may become intense and concentrated, as shown in Fig. 3b. Qualitatively, in this case the gravitational and inertial resistance to sloping ascent vanishes, so that the updraft is relatively vigorous for a given frontogenetical forcing. The downdraft is not enhanced and since upward and downward mass fluxes must still balance, the updraft must be also horizontally restricted, producing the possibility of a mesoscale band of precipitation.

As to the latter mechanism, Bennetts and Hoskins (1979) and Emanuel (1979) have suggested symmetric instability in saturated air as an explanation for band organization. Emanuel (1983a,b) has recently elaborated on the theory and measurement of some integral properties of this phenomenon, which we might refer to as "slantwise convection." Because of its relative novelty and possible importance in this case we will give simple illustrations of the evaluation of this instability, in the differential as opposed to the integral sense, especially suitable for evaluation from cross-sections or from individual soundings.

A schematic vertical cross-section normal to geostrophically balanced base-state flow, with vertical shear in the direction of the flow, appears in Fig. 4. The speed of this flow, $\bar{v}$, is chosen to increase with elevation and to be independent of x, the horizontal direction in the plane of the section. The air is everywhere saturated. Following Emanuel (1983a), we show the distribution of $\bar{M} \equiv \bar{v} + fx$ increasing to the right (since f is taken positive) and increasing upward. Since there is no horizontal pressure-gradient force in the y-direction and since we take no account of viscous effects, $\bar{M} \equiv \bar{v} + fx$ is conserved for an individual displaced parcel (or perhaps better a displaced tube extending indefinitely in the y-direction). We choose a stratification in which the equivalent potential temperature of the base state θ_e increases upward. We assume thermal wind balance. Thus θ_e increases to the right since, following Emanuel (1983a) and Durran and Klemp (1982)

$$\frac{\partial \bar{v}}{\partial z} = \frac{g}{f}\frac{\Gamma_m}{\Gamma_d}\frac{\partial \ln \bar{\theta}_e}{\partial x} \tag{1}$$

where Γ_m and Γ_d are the saturated- and dry-adiabatic lapse rates. Since we assume moist-adiabatic thermodynamics, θ_e is conserved for a displaced parcel.

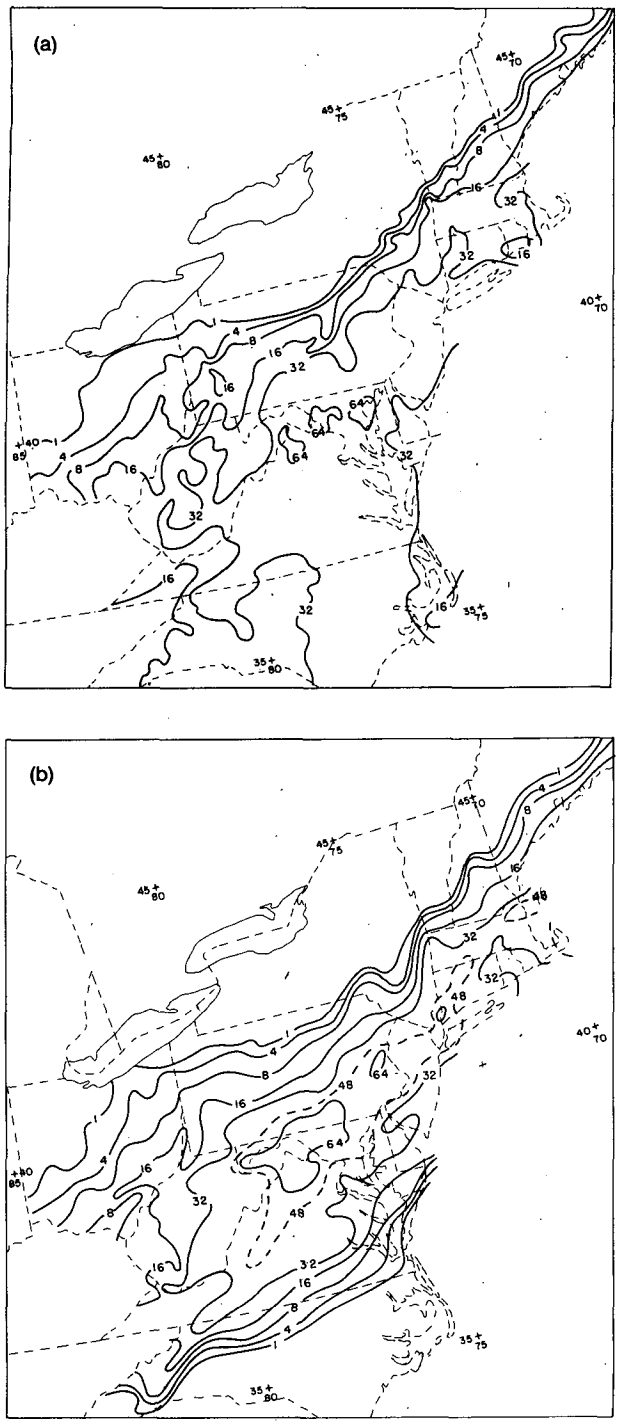

FIG. 2. Total precipitation 10–12 February 1983: (a) total rain and/or equivalent liquid depth of frozen precipitation (mm); (b) depth of snowfall (cm).

Accelerations for a displaced parcel in the x- and z-directions in this case (neglecting the effects of pressure perturbations associated with the displacement are, respectively,

$$\frac{du}{dt} = f[M - \bar{M}] \equiv fM', \tag{2}$$

$$\frac{dw}{dt} = g\left[\frac{\theta - \bar{\theta}}{\bar{\theta}}\right] \equiv \frac{g\theta'}{\bar{\theta}} = g\left[\frac{\theta'_e}{\bar{\theta}_e} - (\exp Q' - 1)\right] \tag{3}$$

where $Q' \equiv Lq'/c_pT$. (For practical purposes $\theta' \approx \theta'_e/2$ for much of the observed range of saturated atmospheric conditions in the middle troposphere. It approaches 0.2 in warm air near the surface and unity in cold upper-tropospheric conditions.) It is readily seen from Fig. 4 that purely horizontal or vertical displacements, shown schematically by points A and B, are stable. For point A, for example, a leftward horizontal displacement produces an excess of parcel M over background $\bar{M}$. Hence $M' > 0$ and from (2) $du/dt > 0$. That is, the horizontal acceleration is to the right, so as to restore the parcel to its initial position. In this case the displayed parcel is positively buoyant, since $\theta_e > \bar{\theta}_e$. The resulting upward acceleration, however, does not mitigate the horizontal acceleration back to the point of origin and does not continue as the thermal stratification is stable; $\partial\bar{\theta}_e/\partial z > 0$. Analogous consideration of the case of vertical displacement, illustrated by point B, also shows stability. For the displaced parcel, $\theta_e < \bar{\theta}_e$ so that the resulting vertical component of acceleration is downward, toward the level of origin. In this case $M < \bar{M}$ for the displaced parcel; thus $M' < 0$ and $du/dt < 0$. However, this horizontal acceleration does not affect the stable downward vertical acceleration and quickly lessens because the momentum structure is inertially stable; $\partial\bar{M}/\partial x > 0$.

Note, however, that the slantwise displacement for point C, with a slope intermediate between those of the $\bar{M}$- and $\bar{\theta}_e$-isopleths, is unstable, i.e., M' and θ'_e have the same sign as the x- and z-components of the displacement, so that the resulting acceleration has a component in the direction of the displacement. It can be seen that slantwise instability requires the slopes of the $\bar{M}$-surfaces to be shallower than those of the $\bar{\theta}_e$-surfaces. From elementary geometrical considerations, the slope of an $\bar{M}$-surface in the z–x plane can be expressed by

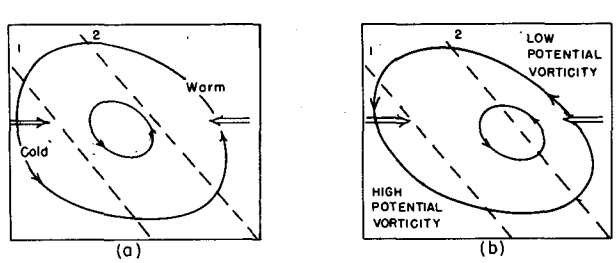

FIG. 3. Vertical cross sections of idealized transverse circulations accompanying large-scale frontogenetical confluence (double-shafted arrows): (a) uniform potential vorticity and (b) vanishing potential vorticity in warmer air. Dashed lines are potential isotherms.

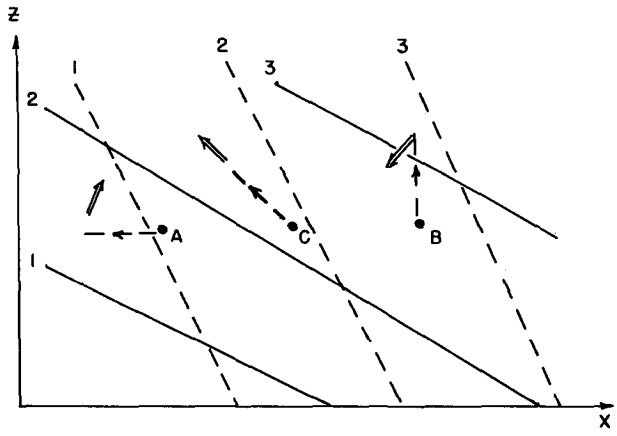

FIG. 4. Schematic vertical cross section illustrating symmetric instability. Solid lines represent absolute momentum $\bar{M}$ of basic flow. Dashed lines represent equivalent potential temperature. Lettered points show sample displacements (dashed) and accelerations (arrowheads). See text.

$$\left(\frac{\delta z}{\delta x}\right)_{\bar{M}} = -\frac{\partial \bar{M}/\partial x}{\partial \bar{M}/\partial z}.$$

From the definition of $\bar{M}$, this slope is given by

$$\left(\frac{\delta z}{\delta x}\right)_{\bar{M}} = -f + \frac{\partial \bar{v}/\partial x}{\partial \bar{v}/\partial z}.$$

Similarly, the slope of a $\bar{\theta}_e$-surface can be expressed by

$$\left(\frac{\delta z}{\delta x}\right)_{\bar{\theta}_e} = -\frac{\partial \bar{\theta}_e/\partial x}{\partial \bar{\theta}_e/\partial z}.$$

From the thermal-wind relationship (1) this latter slope can also be expressed as

$$\left(\frac{\delta z}{\delta x}\right)_{\bar{\theta}_e} = -\left(\frac{\bar{\theta}_e}{g}\right)\left(\frac{\Gamma_d}{\Gamma_m}\right) f \frac{\partial \bar{v}/\partial z}{\partial \bar{\theta}_e/\partial z}.$$

The condition that the $\bar{M}$-surfaces be shallower than the $\bar{\theta}_e$-surfaces is that

$$\frac{(\delta z/\delta x)_{\bar{M}}}{(\delta z/\delta x)_{\bar{\theta}_e}} = \left(\frac{\bar{\eta}}{f}\right)\left(\frac{\Gamma_m}{\Gamma_d}\right)\frac{g}{\bar{\theta}_e}\frac{(\partial \bar{\theta}_e/\partial z)}{(\partial \bar{v}/\partial z)^2} \equiv \mathrm{Ri}_{sc} < 1 \quad (4)$$

where $\bar{\eta} = f + \partial \bar{v}/\partial x$ is taken as the absolute vorticity and Ri_{sc} has been introduced because it seems reasonable to refer to the ratio as the "Richardson Number for slantwise convection." Another way of viewing the criterion for instability is obtained by noting that if the slope of the $\bar{M}$-surfaces is shallower, with $\bar{M}$ increasing upward, then $\bar{M}$ decreases in the positive x-direction along a $\bar{\theta}_e$-surface. From the definition of $\bar{M}$, this is equivalent to stating that

$$\left(\frac{\partial \bar{v}}{\partial x} + f\right)_{\bar{\theta}_e} = \bar{\eta}_{\bar{\theta}_e} < 0.$$

The importance of negative absolute vorticity along $\bar{\theta}_e$-surfaces in the stimulation of inertial motions was discussed by Bjerknes (1951), but in the context of an amplifying synoptic-scale circulation rather than smaller-scale instability.

Finally, we should note that the coefficient, $g/\bar{\theta}$, in (3) is about 300 times larger than the middle-latitude coefficient f in (2). Therefore, unless θ', and thus θ'_e, are extremely small the vertical acceleration will utterly dominate the horizontal one. Equivalently, the motions will tend to be nearly along the $\bar{\theta}_e$ surfaces.

3. Measurements of frontogenetical forcing and evidence for symmetric instability

a. Vertical cross section, 1200 GMT 11 February

The gross structure of the troposphere north of the surface cyclone at an early stage of the storm's impact upon megalopolis is illustrated in Fig. 5. The flow was broadly frontogenetical, since there was warm advection everywhere south of the 876-decameter

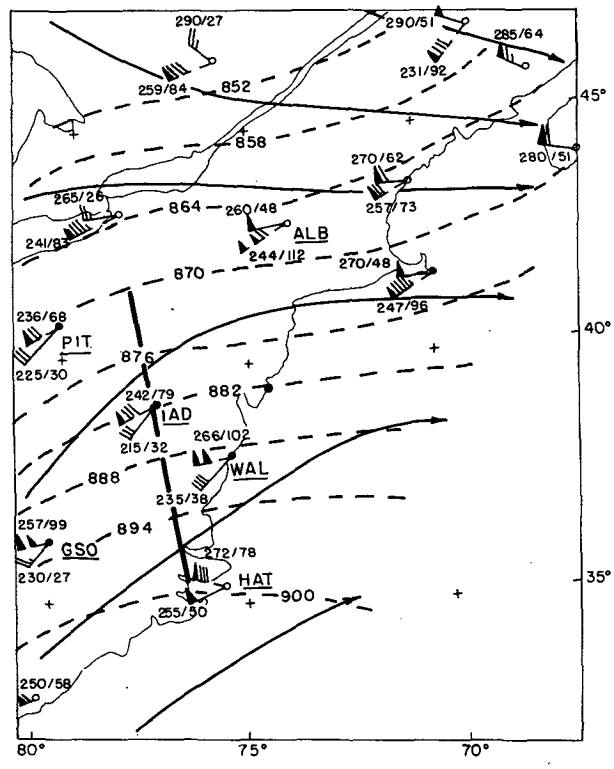

FIG. 5. Contours at 500 mb (solid lines, at intervals of 6 dam) and thickness of the layer from 850 to 250 mb (dashed lines, at intervals of 6 dam). Plotted winds for 500 mb (solid shaft) and for shear from 850 to 250 mb (dashed shaft). Each pennant, full barb and half barb corresponds to 25, 5 and 2.5 m s^{-1}, respectively. (Plotted numbers denote direction in degrees and speeds in knots.) Filled station circles indicate dew-point depression less than 5°C. Heavy line shows position of cross section in Fig. 18. For 1200 GMT 11 February.

(dam) thickness line and cold advection north of the adjacent 870-isopleth. Winds at 500 mb and wind shears over the layer were not far from geostrophic balance except at ALB, where the data were extrapolated from a sounding that failed below the 250 mb level and may have been wrong. Within the layer, however, we shall find a prominent ageostrophic circulation.

To illustrate the structure in more detail, we projected the soundings from PIT, IAD, WAL and HAT on the cross-section line shown in Fig. 5 oriented 345–165°, normal to the thermal wind in the layer from 850 to 250 mb. Analyses of the field of equivalent-potential temperature θ_e and of the estimated area of saturation (derived from rawinsonde humidities, surface observations and satellite imagery) appear in Fig. 6a. Except at HAT the vertical structure of the θ_e-field shows four layers: a reasonably well-mixed surface boundary layer 75 to 100 mb deep, a stable layer extending upward to the middle troposphere, a layer with small conditional stability occupying the middle to upper troposphere, and the stable stratosphere above a tropopause between 250 and 300 mb. The air was at, or close to, saturation throughout and snow was observed at the ground, with moderate intensity at IAD. At HAT a more complicated structure was observed, with a number of relatively thin layers of saturated air and with potential instability for parcels originating in the thin stratum of high θ_e just above an ocean-cooled surface layer. The schematic cumulus cloud is based on this instability and on the observation of occasional moderate rain at HAT at 1100 GMT. The edge of the deep cloud between WAL and HAT is estimated from satellite IR imagery.

The motion in the plane of the section is approximated by the mass streamfunction ψ^x shown in Fig. 6b. It is defined by

$$\psi^x(p) \equiv \int_p^{p_s} u\,dp$$

where p_s is pressure at the surface and u is the wind component from 345°. The x-axis is taken toward the right in the plane of the section, for consistency with Fig. 4. The ψ^x-field represents u exactly.

As for the vertical motion, consider the equation of continuity of mass in a cartesian frame

$$\omega(p) \equiv \frac{dp}{dt} = \int_p^{p_s} \left(\frac{\partial u}{\partial x} + \frac{\partial v}{\partial y}\right) dp = \frac{\partial \psi^x}{\partial x} + \frac{\partial \psi^y}{\partial y} = \omega^x + \omega^y$$

where

$$\psi^y \equiv \int_p^{p_s} v\,dp; \quad \omega^x \equiv \frac{\partial \psi^x}{\partial x}; \quad \omega^y \equiv \frac{\partial \psi^y}{\partial y}.$$

In the present case, owing to the elongation of the precipitation area from east-northeast to west-southwest, and to the previously mentioned frontogenetical character of the synoptic-scale flow, we assume that ω^x, which can be obtained from the streamfunction field shown in Fig. 6b, is larger than ω^y and represents the total vertical-motion field reasonably well, at least in the lower and middle troposphere. This picture will exaggerate the ascent, since with the confluent flow, $\partial v/\partial y > 0$. An estimate of ω^y can be obtained by assuming that $\partial v/\partial y$ is approximately given by $-\partial u_g/\partial x$, u_g being the geostrophic value to be obtained later for another purpose. Resulting values of ω^y at selected points are also shown in Fig. 6b.

In this diagram, ω^x shows a strong sloping updraft along the transition zone at the base of the layer of small conditional stability. Its horizontal half-width was about 100 km. Maximum ascent was found in the middle and upper troposphere near IAD, where the heaviest snowfall was observed at this time. At 200 mb, in the lower stratosphere where the vertical motion should be slight, the correction produced by w^y removes most of the ascent from ω^x. This correction reduces the maximum ascent near the 600 mb level by about 20%. (The corrected kinematical vertical motion is between 20 and 30 cm s^{-1} in the major updraft on 100 km scale between the 700 and 300 mb levels.) The descent above 600 mb over and northwest of HAT corresponds to a region of very dry air above 550 mb observed there. The correction fails to remove the pronounced descent at 200 mb, which must be regarded as spurious, possibly owing to unreliability of the geopotential analysis over the ocean, from which the correction was derived.

For assessment of the possibility of symmetric instability, Fig. 6c combines the fields of θ_e and $M_g \equiv v_g + fx$. The latter quantity was calculated by multiplying $f(9 \times 10^{-5}\ s^{-1})$ by the distance along the section to the right of PIT and adding v_g, the component of geostrophic wind into the plane of the section, measured by differencing the geopotential over distances of about 200 km along the section from a series of analyses at standard pressure levels. In the context of the preceding section, M_g is identified with $\bar{M}$. The geostrophic value must be used because $\bar{M}$ contains a representation of the horizontal pressure-gradient force through $\bar{v}$, which is assumed to be in geostrophic balance. We see in Fig. 6c a region of slantwise instability in the region of small hydrostatic stability in the upper troposphere between PIT and WAL. An extension of small or negative slantwise stability to lower levels is seen at WAL. This region is downwind in the large-scale flow from a region of modest latent instability for upright convection, as documented by the soundings at HAT and at GSO (not shown). If we visualize a trajectory in the large-scale flow, perhaps ordinary convection occurs first,

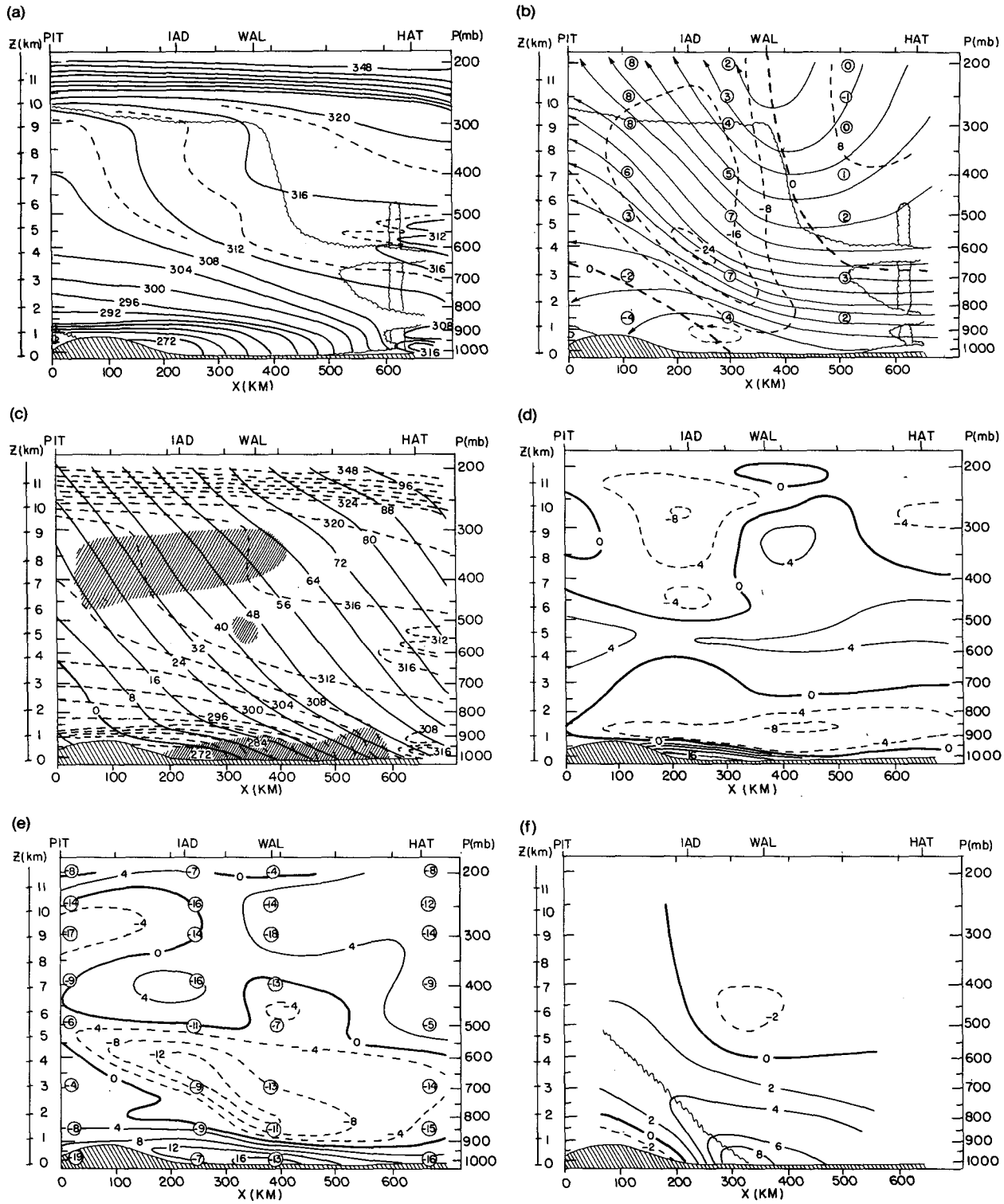

FIG. 6. Vertical cross sections PIT–HAT, 1200 GMT 11 February 1983. (a) Equivalent-potential temperature at intervals of 4 K, with schematic cloud mass indicated by scalloped line. (b) Streamfunction ψ^x (solid lines, at intervals of 8×10^2 mb m s^{-1}) and vertical motion, ω^x (dashed lines at intervals of 8×10^{-3} mb s^{-1}). Circled numbers are estimates of ω^y. See text. Cloud outline added. (c) Absolute geostrophic momentum M_g (solid lines, at intervals of 8 m s^{-1}) and equivalent-potential temperature (dashed), as in (a). Shading denotes areas of symmetric instability. (d) Ageostrophic v-component (m s^{-1}, from 255°). (e) Ageostrophic u-component (m s^{-1}, from 345°). Circled numbers are geostrophic u-components. (f) Geostrophic frontogenesis, $-(\partial u_g/\partial x)(\partial T/\partial x)$, at intervals of 2×10^{-5} K (100 km)$^{-1}$ s^{-1}. Jagged line shows axis of maximum frontogenesis.

removing the irregularities in the θ_e-profile and leaving a nearly neutral stratification with sufficient vertical wind shear to make the structure symmetrically unstable. A third region where the M_g-isopleths are shallower than the θ_e-isotherms is the lowest kilometer over most of the section. Our inviscid mechanism, however, does not seem applicable to this region, where the surface viscous force is surely important. It is noteworthy that thunderstorm activity described by Bosart and Sanders (1985) broke out not far from IAD, in a region where there was no evidence of buoyancy for conventional upright convection, but where a deep atmospheric layer displayed slight or negative symmetric stability.

The practical application of (4) to individual soundings requires association of the vertical shear of the observed wind with the shear of the geostrophic wind. The reliability of this association can be gauged by an examination of the ageostrophic v-components, which are shown in Fig. 6d. The largest values are within or immediately adjacent to the surface boundary layer. Above this, a patchy pattern with maximum magnitudes near 4 m s^{-1} probably represents errors in the observations or analysis and small-scale variability not adequately resolvable in the routine data. These results constitute a warning that shallow layers of observed wind shear indicating slantwise instability should be regarded with caution.

The applicability of the idealized section in Fig. 4 must be questioned because the basic flow was not in the same direction as the thermal wind, as seen for example in Fig. 5. The conservation of M is based on the premise of no force, or more generally no *net* force, in the y-direction. If the u-components of motion are not in geostrophic balance then there is a net force in the y-direction. Hence it is desirable to estimate the ageostrophic u-components. They appear in Fig. 6e, displaying a prominent circulation below 500 mb, positive (from cold to warm) in potentially cold air near the ground and negative (from warm to cold) in potentially warmer air above. Maximum magnitudes were in excess of 12 m s^{-1} and the dividing line sloped upward toward the northwest, from 940 mb near HAT to 700 mb between IAD and PIT. This circulation constituted the horizontal limb of the vigorous pattern of ascent shown in Fig. 6b. Above 500 mb a patchy cellular pattern is seen, with maximum values near 4 m s^{-1}. Little significance is attached to this pattern. In much of this upper region, then, the net force in the y-direction was relatively small, and the finding of low symmetric stability seems defensible.

There is a clear indication in Fig. 6b of an intense transverse frontal circulation below 500 mb. Moreover, the geostrophic u-components, appearing in Fig. 6e, showed pronounced lower-tropospheric confluence. We calculated the geostrophic frontogenetical forcing $-(\partial u_g/\partial x)(\partial T/\partial x)$ from

$$-\frac{\partial u_g}{\partial x}\frac{\partial T}{\partial x} = \frac{pf}{\rho}\frac{\delta u_g}{\delta x}\frac{\delta v_g}{\delta p}$$

where δx and δp were taken as 200 km and 100 mb, respectively. The results appear in Fig. 6f. There was a broad zone of frontogenesis with central intensity of several °C (100 km)$^{-1}$ per day. Maximum strength was at the ground near WAL, extending upward and northwestward to the 500 mb level between PIT and IAD. Frontolytical forcing occurred above 600 mb southeast of IAD.

Comparing Figs. 6e and f, we see that the axis of maximum geostrophic frontogenesis lay near the maximum positive ageostrophic u at the ground but extended up into negative values above 800 mb. Maximum negative ageostrophic u occurred about 100 km from the axis of frontogenesis, toward the warmer air. Comparing Figs. 6b and f, we see that maximum ascent occurred in a band nearly parallel to the axis of frontogenesis, being displaced horizontally about 100 km from it, toward the warmer air, and about 200 mb (2.5 km) above it. This structure strongly resembles a recent theoretical result of Emanuel (1985), from a diagnostic semigeostrophic model with a discontinuity in potential vorticity. The discontinuity is along a line parallel to, and some distance toward the warmer air from, the axis of maximum frontogenesis. Positive values below this line drop to zero above it. In the present case, the region of small potential vorticity (cf. Fig. 6c) lies above the frontogenetical axis, consistent with the model structure.

We conclude that at this time the intense updraft seen over IAD in Fig. 6b was a concentrated response to large-scale frontogenetical forcing. The intensity and size in the mesoscale range is attributable to low symmetric stability in the warmer air, while symmetric instability *per se* may have produced structure in the upper portion of the cloud system without having a large effect upon precipitation at the surface.

b. Vertical cross section, 0000 GMT 12 February

Twelve hours later, the surface low had moved northeastward to a position about 100 km southeast of WAL (Fig. 1b). Heavy snow had advanced into southwestern New England. The synoptic-scale structure is further illustrated in Fig. 7. The flow was again broadly frontogenetical, this time east of longitude 75°W. That is, there was pronounced warm advection south of the 876 dam thickness line, vanishing along and north of the 870 dam line. The vertical shear of the wind crossed the thickness lines at a substantial angle and was much stronger than required for thermal wind balance. The flow over New England displayed marked anticyclonic curvature at and above the 500 mb level.

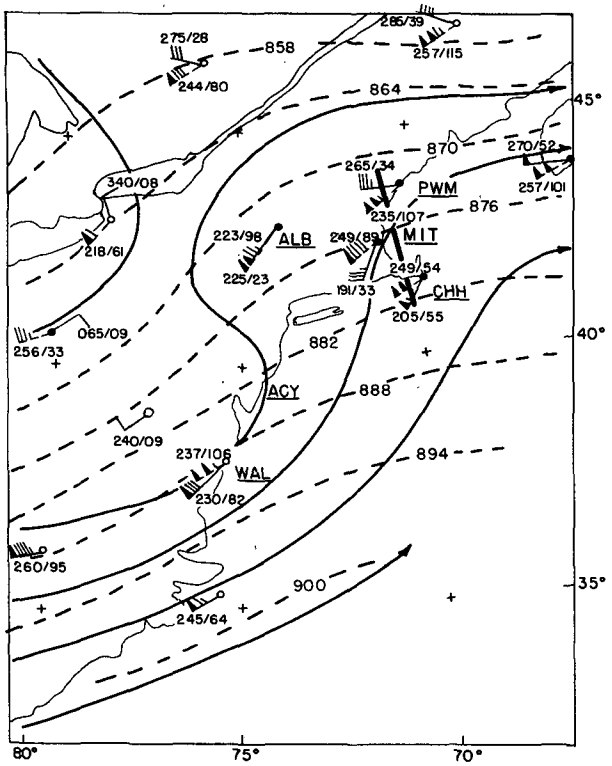

FIG. 7. As in Fig. 5 except for 0000 GMT 12 February 1983. Heavy line shows position of cross section in Fig. 8.

The best choice of stations for cross-section analysis was the trio, PWM, MIT, and CHH, which were projected on a line oriented 350–170° (normal to the thickness lines) shown in Fig. 7. A set of analyses analogous to those discussed earlier are presented in Fig. 8.

The field of θ_e (Fig. 8a) shows the same four main features seen in Fig. 6a; namely, a well-mixed surface boundary layer about 1 km deep, then a stable layer extending through about the next 1.5 km, and then a deep layer of small conditional stability for upright convection reaching up to the tropopause and a very stable lower stratosphere. Three points of difference deserve note. First, the tropopause was nearly 50 mb higher and was sharper than on the earlier section. These modifications are probably attributable to the vigorous upper-tropospheric ascent discussed earlier. Second, a sloping layer of relatively stable air was embedded between 500 and 400 mb in the low-stability region. This layer was associated with extraordinarily strong vertical wind shear, as we will see. Finally, the cloud structure was different. The major cloud mass associated with the storm was based for the most part near the top of the stable layer. Below this mass the air was very dry, except in the mixed layer, which contained low clouds in much of the area between MIT and CHH. Light snow flurries had been falling from this cloud deck for many hours.

The pattern of streamfunction ω^x in Fig. 8b shows weak flow below the 550 mb level shearing strongly through the stable layer discussed before, with strong southerly components up through the middle and upper troposphere. The vertical motions, even after application of the large estimated corrections for ω^y, show strong ascent above 500 mb between PWM and MIT, comparable to the maximum ascent on Fig. 6b. One might doubt the credibility of this ascent, since it was not producing snow at the ground, and MIT radar detected the major snow band about 50 km south of CHH at this time. However, the cloud base lay about 2 km beneath the active ascending flow and most likely marked the lower limit of evaporating snow falling from above. Moreover, satellite IR imagery at this time showed a separate area of high cold clouds in the region of ascent, moving rapidly northeastward and becoming detached from the main cloud mass to the southwest. (The time track of this surge appears in Fig. 10.) Hence it seems that this ascent was an isolated pulse at high levels, preceding the major storm.

Prospects for slantwise convection within the main cloud mass can be estimated from Fig. 8c, displaying the fields of θ_e and M_g, taken this time from the geostrophic component from 260°. Symmetric stability was weak throughout this mass, with small unstable regions arising because of minor irregularities in the profile of θ_e between MIT and CHH and because of strong anticyclonic shear between PWM and MIT. The boundary-layer cloud displayed inviscid instability but, as before, the interpretation is difficult.

The pattern of ageostrophic v-component (Fig. 8d) below the 500 mb level was similar to that described earlier (Fig. 6d). Above, however, substantial positive values dominated. This supergeostrophic speed into the plane of the cross section confirms that trajectories, as well as streamlines, were anticyclonically curved in the middle and upper troposphere. The perturbation at MIT, with a prominent maximum at 400 mb and a minimum at 290 mb, points to the danger of using the vertical shear of the observed wind to evaluate the symmetric stability.

In the field of ageostrophic u-component shown in Fig. 8e there was a transverse circulation near the 500 mb level, from colder to warmer air (positive) below and opposite above. Substantial negative values extended upward to the tropopause, in contrast to the pattern 12 hours earlier (Fig. 6e). Positive values extended from the transition level down to the ground, so that the vertical shear through the entire troposphere contained a strong component from warmer toward colder air at this time, as noted above. It was seen that confluence in the u_g-components dominated the section and was especially intense in the middle troposphere.

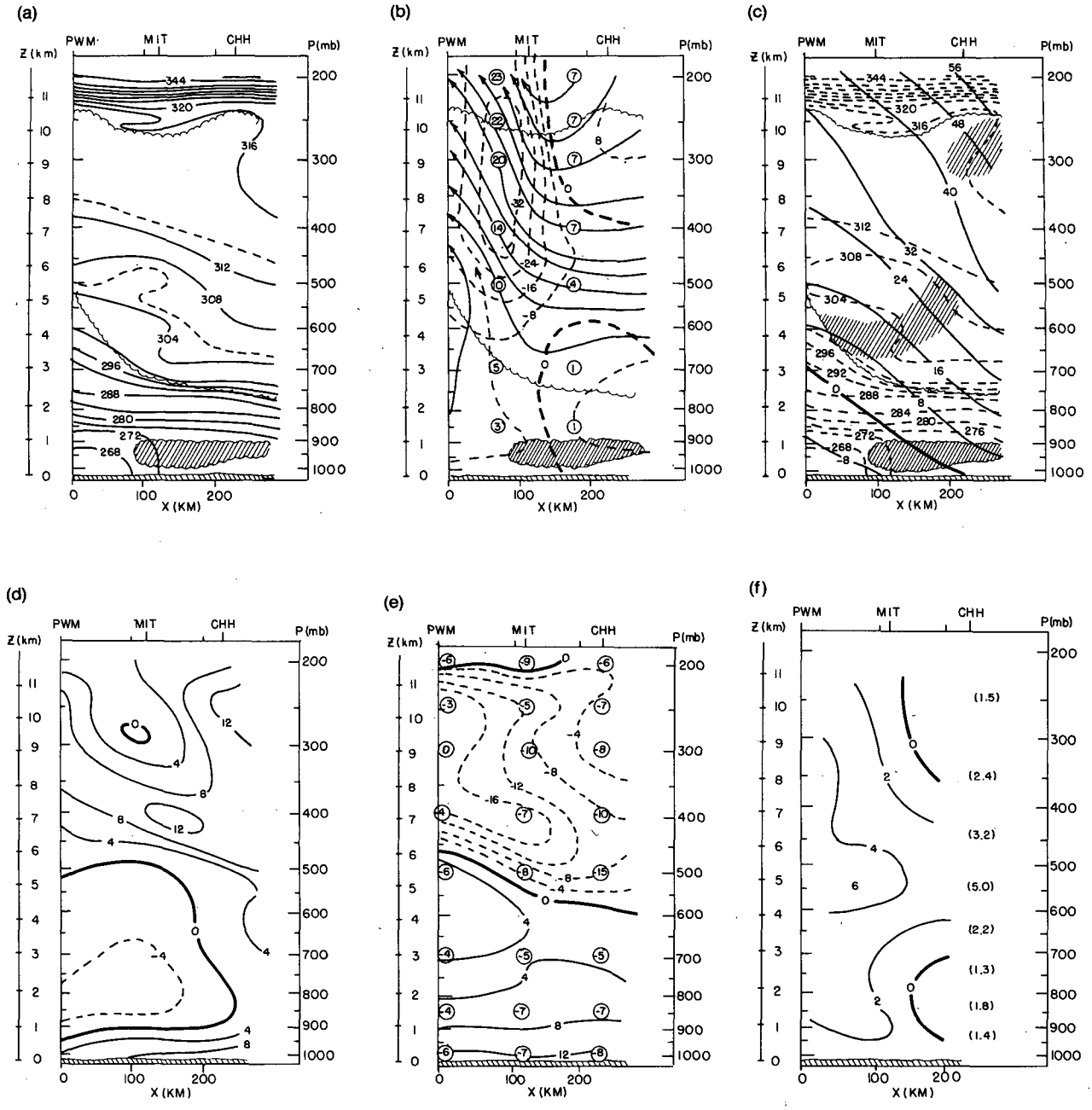

FIG. 8. As in Fig. 6 but for vertical cross sections PWM–CHH, 0000 GMT 12 February 1983.

Accordingly, the geostrophic frontogenetical forcing, $-(\partial u_g/\partial x)(\partial T/\partial x)$, was computed as before, except that δx was taken as 100 km to accommodate the closer spacing of stations. The results appearing in Fig. 8f included additional values calculated for δx = 200 km to facilitate comparison with Fig. 6f. Frontogenesis was positive on this occasion throughout almost the entire section. Maximum values occurred near the 550 mb level rather than near the ground as in Fig. 6f, but magnitudes were comparable. Comparison of Figs. 8b, e and f shows similar relationships among frontogenetical forcing, ageostrophic u-component, and vertical motion, the first lying about 2.5 km below the other two.

In summary, as 12 hours earlier, we see at this time a pronounced ageostrophic circulation in response to strong geostrophic frontogenetical forcing. This time, however, the maximum forcing occurred well aloft, in a region of small symmetric stability. The strong ascent produced an elevated region in the

cloud top which moved away from the main cloud system, perhaps as a manifestation of symmetric instability.

c. *MIT sounding, 0600 GMT 12 February*

After 0000 GMT (Fig. 1c) the region of strongest warm advection had moved to the east of New England, and relevant cross-section analysis was not possible. The MIT observation for 0600 GMT (an extraordinarily difficult balloon release in gale-force winds and heavy snow) was highly informative and appears in Fig. 9. In this sounding, the temperature profile was derived from individual contact values and the winds were evaluated as nonoverlapping 3-minute averages. The temperature and wind structures at 0600 GMT show considerable similarity to those seen at MIT at 0000 GMT (Fig. 8). At the later time snow had filled the earlier dry layer between 890 and 730 mb. Winds in the upper troposphere had backed at the later time and the tropopause was lower and much less pronounced.

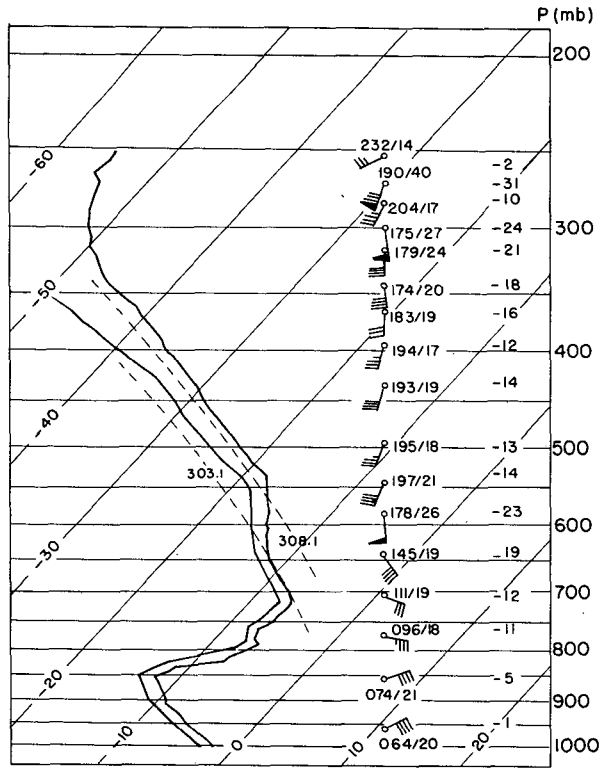

FIG. 9. Rawinsonde observation from MIT for 0600 GMT 12 February 1983, plotted on a Skew T–log p diagram. Solid lines show temperature and dew-point profiles. Plotted winds are also shown by direction and speed in degrees and m s^{-1}. Values to right of wind plots are wind component (m s^{-1}) from 330°, transverse to direction of thermal wind for the layer from 850 to 250 mb, interpreted in time. Saturated adiabats for indicated θ_e values appear as dashed lines.

A layer of relatively large wind shear and stability, embedded in the deep layer of low stability from 700 mb to the tropopause, is seen between 650 and 535 mb, virtually identical to the layer between 500 and 400 mb at the earlier time. The wind signature is a rapid upward increase in the component normal to the synoptic-scale thermal wind (interpolated in time in this instance), from warmer toward colder air, with a maximum near the top of the stable layer. This feature is almost certainly ageostrophic, as seen in Figs. 6e and 8e. A notable difference is the range of θ_e covered: from 306 to 313 K at the earlier time and 303 and 308 K later. The interpretation of this difference is beyond the scope of this paper, but it rules out the possibility of a single frontal layer of uniform θ_e.

d. *Satellite imagery*

The tracks of a number of cold patches in the satellite imagery, thought to reflect the presence of surges of the type suggested in the discussion of Fig. 8, appear in Fig. 10. The more prominent and long-lived areas are designated by letter.

Area A was associated with the strong updraft seen near IAD at 1200 GMT on the 11th. The large-amplitude gravity wave discussed by Bosart and Sanders (1985) was evidently associated with the initiation of C at 1900 GMT and travelled at its southwestern edge until 0000 GMT when the area fragmented. Thereafter, the wave travelled with the southwestern piece, denoted F, until 0600 GMT when it accelerated eastward, perhaps fracturing its easternmost portion at 0800 GMT. The combined entity C–F was by far the most long-lived of its peers and lay along the northeastern edge of the region of heavy snow. Close examination of the satellite imagery showed that this area was more or less continuously fed by generation of new elements just ahead of the gravity wave crest. These elements moved quickly northeastward to merge with the main cold area. This quasi-steady area was evidently associated with the shear layer observed at MIT at 0600 GMT. Returning to the fragmentation of C at 0000 GMT, it appears that the northeasternmost piece, denoted D, was associated with the shear layer at MIT at this time. The fragment E was associated with a stable layer and strong ageostrophic shear in the 0000 GMT sounding from ALB (not shown). The elongation of the cold patches, when pronounced, was more or less along the direction of the thermal wind. The best examples of this characteristic of symmetric instability are B, C and E.

4. Conclusions

We have studied the megalopolitan snow storm of 11–12 February 1983 principally by analysis of rawinsonde data. We find that the concentration of

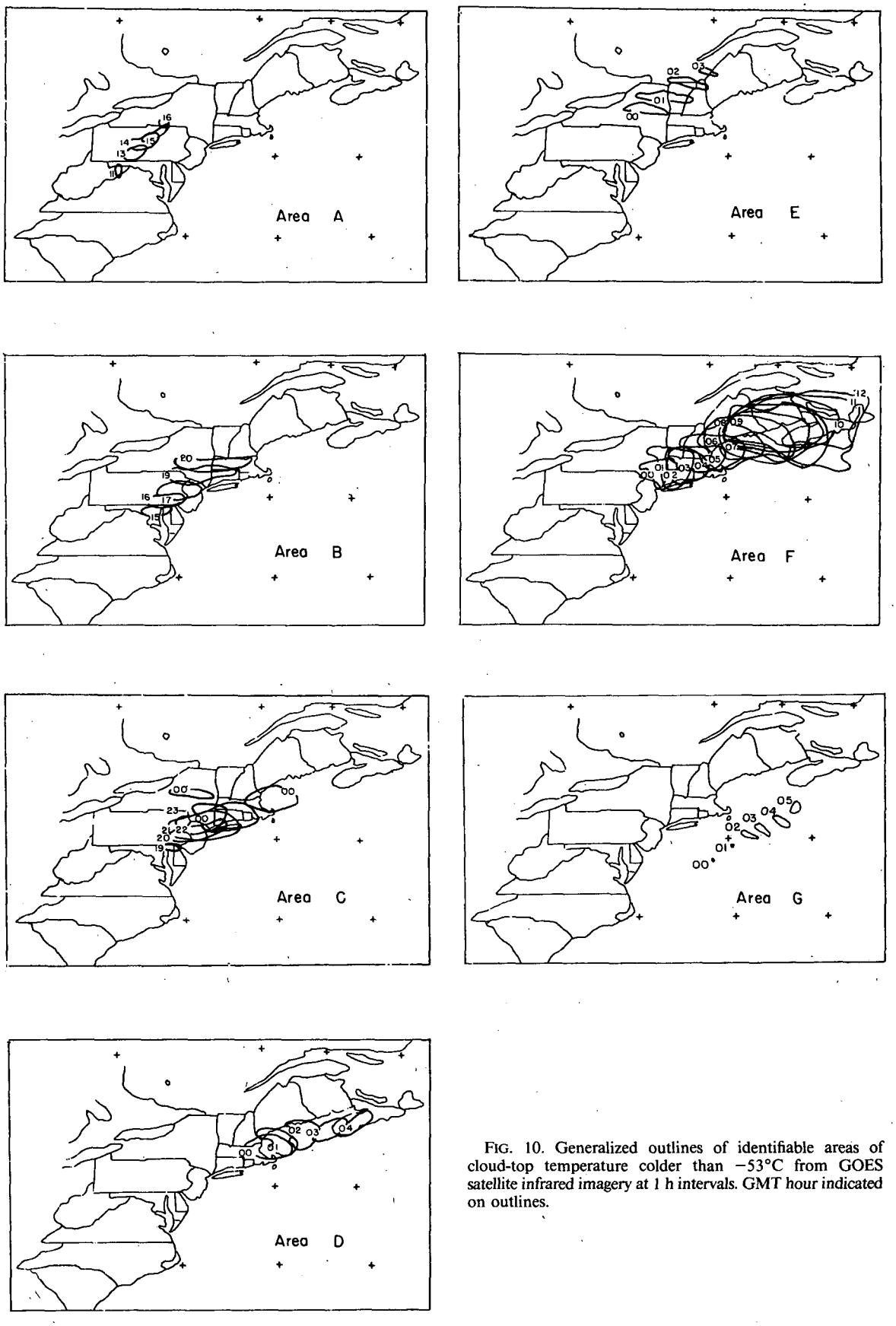

FIG. 10. Generalized outlines of identifiable areas of cloud-top temperature colder than −53°C from GOES satellite infrared imagery at 1 h intervals. GMT hour indicated on outlines.

snowfall in a band parallel to the tropospheric thermal wind is attributable mainly to a prominent thermally direct circulation induced by geostrophic frontogenetical forcing. The ascent was particularly intense owing to small symmetric stability in the saturated warmer air mass, consistent with a theoretical model suggested by Emanuel (1985). Symmetric instability in parts of this air mass appears to be responsible for pulse-like eruptions of elevated cloud top seen in satellite imagery, elongated in the direction of the thermal wind.

Acknowledgment. We very much appreciate discussions with Kerry Emanuel and Rich Passarelli of MIT and Dan Keyser of NASA/GLAS during the course of this research. The vital soundings at MIT were made by an enthusiastic team including graduate students John Nielsen, Steven Garner, Dawn Wolfsberg, Marc Seltzer and Josh Wurman. Thanks are due to Ms. Isabelle Kole for drafting of figures. This research was sponsored by the National Science Foundation under grants ATM-802655703 (SUNYA), ATM-801930 (MIT), and ATM-8209375 (MIT).

REFERENCES

Bennetts, D. A., and B. J. Hoskins, 1979: Conditional symmetric instability—a possible explanation for frontal rainbands. *Quart. J. Roy. Meteor. Soc.*, **105,** 945–962.

Bjerknes, J., 1919: On the structure of moving cyclones. *Geofys. Publikajoner, Norske Videnskaps-Akad.*, Oslo, **1,** 1–8.

——, 1951: Extratropical cyclones. *Compendium of Meteorology,* T. F. Malone, Ed., Amer. Meteor. Soc., 577–598.

Bosart, L. F., and F. Sanders, 1985: Mesoscale structure in the megalopolitan snowstorm of 11-12 February 1983. Part III: A large amplitude gravity wave. *J. Atmos. Sci.*, **42** (to be published).

Brooks, C. F., and I. I. Schell, 1950: Forecasting heavy snowstorms at Blue Hill (Boston), Mass. *Bull. Amer. Meteor. Soc.*, **31,** 131–133.

Durran, D. R., and J. B. Klemp, 1982: On the effects of moisture on the Brunt-Väisälä frequency. *J. Atmos. Sci.*, **39,** 2152–2158.

Eliassen, A., 1959: The formation of fronts in the atmosphere, *The Atmosphere and the Sea in Motion,* B. Bolin, Ed., The Rockefeller Institute Press, 277–287.

Emanuel, K. A., 1979: Inertial instability and mesoscale convective systems. Part I: Linear theory of inertial instability in rotating viscous fluids. *J. Atmos. Sci.*, **38,** 2425–2449.

——, 1983a: The Lagrangian parcel dynamics of moist symmetric instability. *J. Atmos. Sci.*, **40,** 2368–2376.

——, 1983b: On assessing local conditional symmetric instability from atmospheric soundings. *Mon. Wea. Rev.*, **111,** 2016–2033.

——, 1985: Frontogenesis in the presence of low moist symmetric stability. *J. Atmos. Sci.*, **42,** 1062–1071.

Herzegh, P. H., and P. V. Hobbs, 1980: The mesoscale and microscale structure and organization of clouds and precipitation in midlatitude cyclones. Part II: Warm frontal clouds. *J. Atmos. Sci.*, **37,** 597–611.

Heymsfield, G. M., 1979: Doppler radar study of a warm frontal region. *J. Atmos. Sci.*, **36,** 2093–2107.

Hoskins, B. J., and F. P. Bretherton, 1972: Atmospheric frontogenesis models: Mathematical formulation and solution. *J. Atmos. Sci.*, **29,** 11–37.

Houze, R. A., Jr., S. A. Rutledge, T. J. Matejka and P. V. Hobbs, 1981: The mesoscale and microscale structure and organization for clouds and precipitation in midlatitude cyclones. Part III: Air motions and precipitation growth in a warm-frontal rainband. *J. Atmos. Sci.*, **38,** 639–649.

Namias, J., and P. F. Clapp, 1949: Confluence theory of the high tropospheric jet stream. *J. Meteor.*, **6,** 330–336.

Sanders, F., and L. F. Bosart, 1985: Mesoscale structure in the megalopolitan snowstorm of 11-12 February 1983. Part II: Doppler radar study of the New England snowband. *J. Atmos. Sci.* **42,** (in press).

Sawyer, J. S., 1956: The vertical circulation at meteorological fronts and its relation to frontogenesis. *Proc. Roy. Soc. London,* **A234,** 246–262.

U.S. Dept. of Commerce, 1983: *Storm Data,* **25,** No. 2.